Electronic Supplementary Material (ESI) for Nanoscale Advances.

Bifunctional earth-abundant phosphate/phosphide catalysts prepared *via* atomic layer deposition for electrocatalytic water splitting

Jan Rongé [†a], Thomas Dobbelaere [†b], Lowie Henderick [b], Matthias Minjauw [b], Sreeprasanth Pulinthanathu Sree [a], Jolien Dendooven [b], Johan A. Martens [a], Christophe Detavernier [b]

Supporting Information

Methods

Atomic Layer Deposition

Depositions were carried out in a home-built pump-type PE-ALD reactor, shown schematically in Figure 1. The deposition chamber was continuously evacuated by a turbomolecular pump to a base pressure of approx. 4×10^{-6} mbar. Precursor vapors and gases were admitted through computer-controlled pneumatic valves. The TMP (Me_3PO_4, Sigma-Aldrich, 97%), TBF ($Fe(C_5H_5)$-($C_5H_4C(CH_3)_3$), Alfa Aesar, 98%), and $CoCp_2$ ($Co(C_5H_5)_2$, Alfa Aesar) precursor bottles were heated to resp. 45 °C, 75 °C, and 105 °C. TMP and $CoCp_2$ were delivered by their own vapor pressure (reaching approximate pressures of respectively 5×10^{-3} mbar and 1×10^{-3} mbar in the deposition chamber), while TBF was carried by an argon flow. The argon and O_2 gas flows were adjusted to reach a pressure of 5×10^{-3} mbar in the chamber. The temperature of the chamber walls was set to 130 °C, and all precursor tubes leading to the chamber were additionally heated to prevent any precursor condensation.

Remote plasma was generated inductively using a 13.56 MHz RF generator (ENI GHW-12Z) and a matching network leading to a copper coil wrapped around a quartz column. Before igniting the plasma, vapor or gas from the chamber was fed to the column through a gate valve. The plasma power was set to 200 W for the TMP plasma and 300 W for the O_2 plasma, and the impedance matching was tuned to minimize the reflected power on both. The substrates were mounted to a heated copper block, the temperature of which was PID-controlled. Depositions were performed on pieces of standard p-type silicon (100) wafer (for process characterization), silicon wafer coated with platinum (for OER electrocatalysis), or Toray paper (for HER electrocatalysis).

The iron phosphate pulse sequence consisted of: 15 s TMP plasma – pumping – 10 s O_2 plasma – pumping – 30 s TBF vapor – pumping. These pulse times were already optimized in an earlier report.[1] The optimized cobalt phosphate pulse sequence consisted of: 10 s TMP plasma – pumping – 20 s O_2 plasma – pumping – 7 s $CoCp_2$ vapor – pumping. For both processes, pumping times of 20 s were found sufficient to bring residual pressures below 4×10^{-5} mbar, thereby avoiding any CVD side reactions.

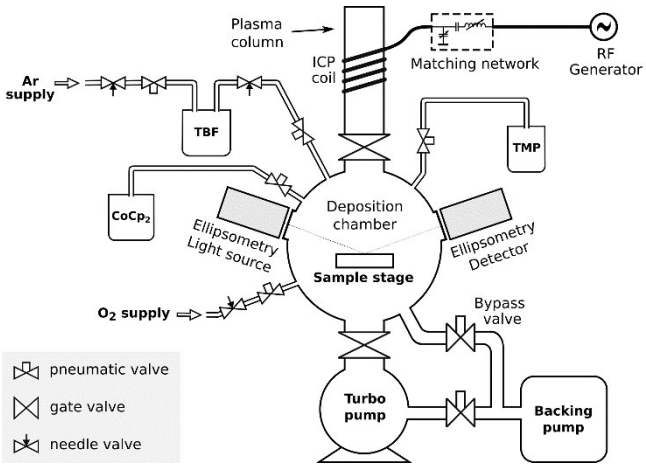

Figure S1: Schematic drawing of the home-made PE-ALD deposition system used to produce the iron and cobalt phosphate films.

Post-deposition annealing

The post-deposition annealing experiments were performed in a home-built setup consisting of a high-temperature stage in a controlled-atmosphere chamber constructed within an X-ray diffractometer (XRD).[2–4] A reducing atmosphere was used, consisting of a mixture of 5% hydrogen in helium; during the annealing process, in-situ XRD patterns could be acquired using a Cu Kα X-ray source and a position sensitive detector.

Phase characterization

Elastic recoil detection (ERD) and Rutherford backscattering spectrometry (RBS) measurements were performed using a Cl^{7+} ion beam with an energy of 43 MeV, impinging under a 10° incidence angle with the sample surface, and recoiled atoms were collected under a 31° scattering angle.

X-ray Photoelectron Spectroscopy (XPS) analysis was performed on a Thermo Scientific Theta Probe XPS instrument using Al Kα X-rays generated at 15 kV and 70 W and focused to a spot size of 0.3 mm by an MXR1 monochromator. The sample surface was etched by Ar^+ ions at an acceleration voltage of 3 keV and a current of 2 µA.

SEM

SEM-images were made with Nova NanoSEM 450 (FEI) using the electron beam with an acceleration voltage (1- 2 kV) and operating in the immersion-lens mode.The samples were immobilized on to an aluminum stub using a carbon sticker and imaged without any further sample modification.

Electrochemical post-deposition treatment and characterization

3-electrode electrochemical voltammetric experiments were performed at ambient temperature using a VersaSTAT 4 potentiostat (Princeton Applied Research) and metal phosphate/phosphide materials deposited on carbon fiber Toray substrate as the working electrode. In some experiments planar Pt layers sputtered onto a Si substrate were used as the working electrode. The contact was made with copper wire and silver glue, and shielded from the electrolyte by an epoxy coat. A graphite counter electrode was used, separated by the working electrode compartment by a glass frit and separately purged with nitrogen during measurements. A calibrated Ag/AgCl (3 M KCl, sat. AgCl, Radiometer Analytical) was used as the reference electrode and inserted in a separate

compartment with a Luggin capillary. 0.1 M KOH or 0.5 M H_2SO_4 was used as the electrolyte. The solution was vigorously stirred with a magnetic stirrer while purging oxygen (for OER) or hydrogen (for HER) through the solution for at least 10 minutes before and during every experiment.

For every sample, the same experimental procedure was followed: after immersing the sample in the electrolyte and purging for 10 minutes, 5 consecutive cyclic voltammetry scans were run at 100 mV/s scan rate. Next, staircase voltammetry was performed at 10 mV/step and 1 mV/s. This procedure was sufficient to activate the samples. Further electrochemical treatments did not result in better performance.

Reported data were corrected for the uncompensated resistance (R_u) and current densities were normalized to the geometric surface area. R_u was determined by performing potentiostatic (at 0 V vs open circuit) and galvanostatic (at 10 mA/cm^2) impedance spectroscopy in a frequency region between 1 Hz and 1 MHz. R_u was extracted from the data by taking the real part of the impedance in the high frequency region where phase angle was zero. R_u was similar for potentiostatic and galvanostatic measurements. Geometric areas were determined by making a photograph of the electrode and using the software ImageJ to calculate the area. The measured potentials were converted to the potentials against the reversible hydrogen electrode (RHE).

TOF calculation

Turnover frequencies (TOF) were calculated using the following equation:

$$TOF = FE \cdot i / (2\ F\ n)$$

Where FE is Faradaic Efficiency, i is the current density (A/cm^2), F Faraday constant (C/mol) and n the metal loading (mol/cm^2), which was determined from XRF results. For cobalt phosphate, a layer thickness of 74 nm was found by XRF, corresponding with 24 µg/cm^2 at a material density of 3.2 g/cm^3. Similarly, for iron phosphate a loading of 34 µg/cm^2 was obtained. Note that a FE of 100% was assumed. This was not explicitly measured, but assumed based on existing work that showed 100% FE for phosphide materials in acid medium[5–8]. Goryachev et al. showed that FE may drop for unstable electrodes which dissolve when not under cathodic protection.[9] Cobalt based materials used for HER under acid conditions in this work showed very good stability, but the stability of iron based materials is not warranted (Fig. S7).

Supplementary figures

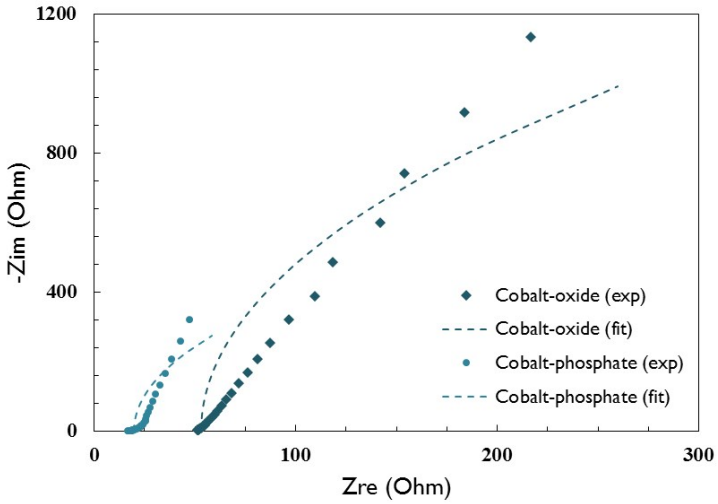

Figure S2: Potentiostatic electrochemical impedance spectroscopy (0 V vs open circuit) of cobalt-oxide and cobalt-phosphate samples after OER activity measurements in 0.1 M KOH, in the frequency range 10 kHz – 10 Hz. Dashed curves show the result of a simplified Randles circuit fit. The fitted capacitance was 55 µF/cm² for the cobalt-oxide sample and 1047 µF/cm² for the cobalt-phosphate sample.

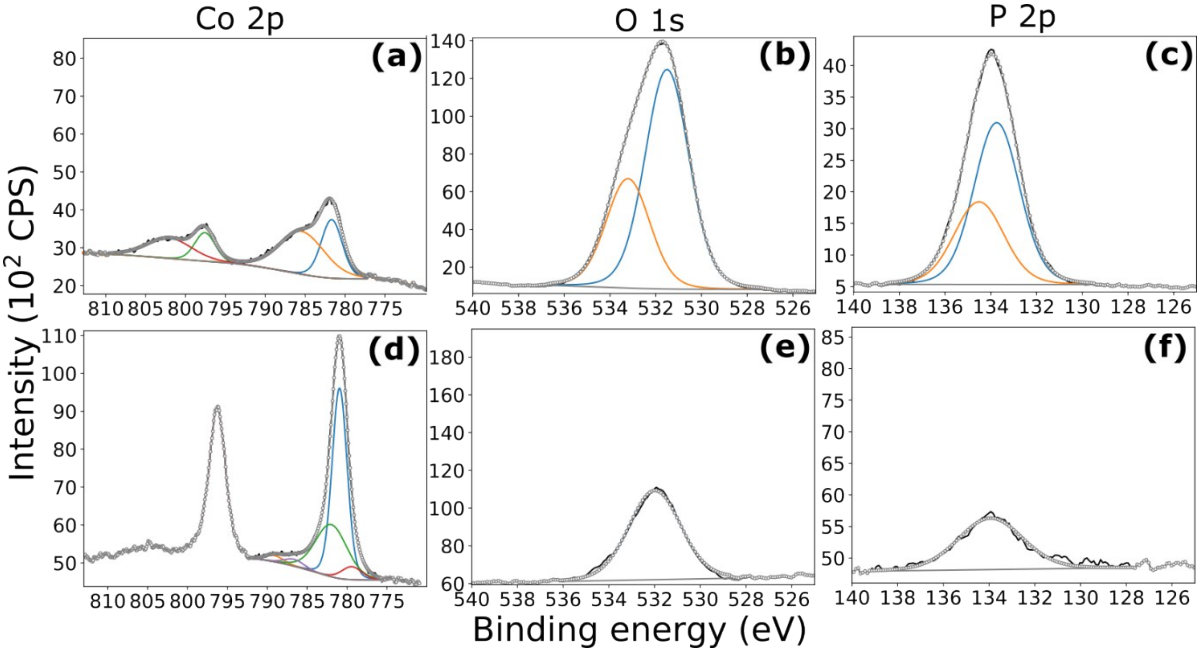

Figure S3: XPS spectra of Co 2p, O 1s and P 2p regions of as-deposited (a-c) and post-OER (d-f) cobalt phosphate material. Figure (a) suggests the presence of Co(II) species, with a main peak at 781.9 eV and the presence of a satellite peak at 785.5 eV. After OER (d), the satellite peaks disappear and Co is at a higher oxidation state. Phosphorus is present as P(V) (c,f).

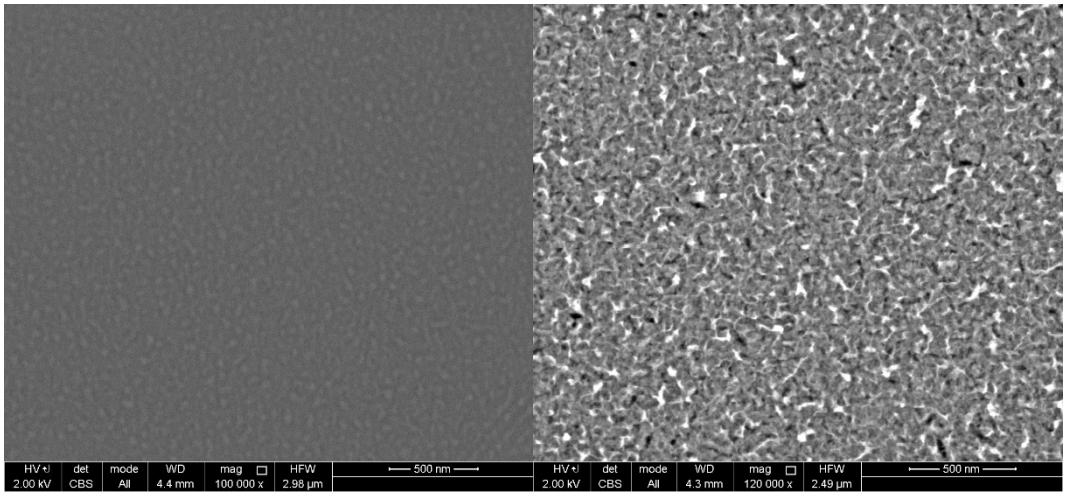

Figure S4: SEM images of as-deposited (left) and post-OER (right) cobalt phosphate material on a silicon wafer coated with Pt by sputtering.

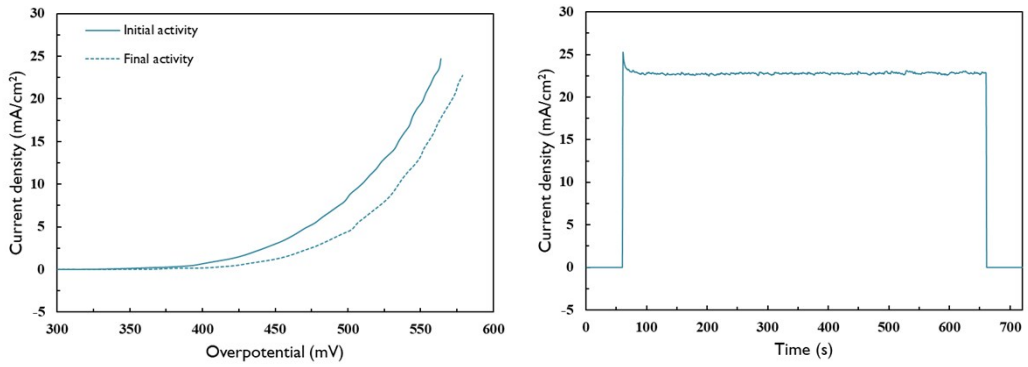

Figure S5: (left) staircase cyclic voltammetry of ALD as-deposited cobalt phosphate in 0.1 M KOH, before and after OER measurements. Measurements included slow and fast cyclic voltammetry, chronoamperometry and chronopotentiometry. Right figure shows catalytic current at an applied potential of 1.81 V vs RHE, for the same sample.

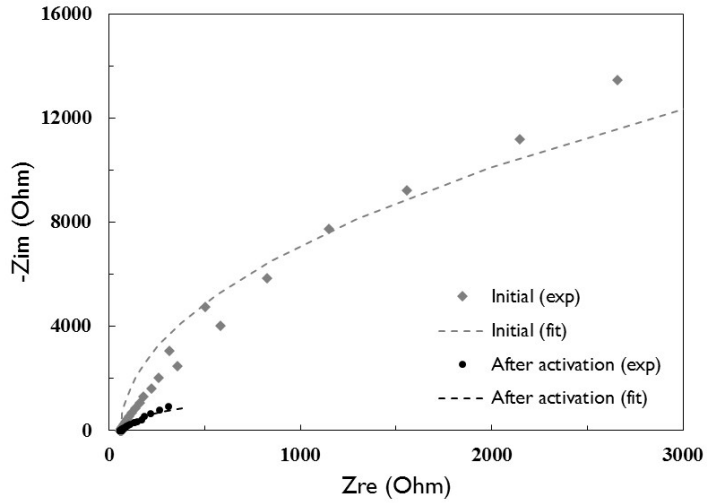

Figure S6: Potentiostatic electrochemical impedance spectroscopy (0 V vs open circuit) of cobalt-phosphate sample before (as-deposited) and after reductive activation in 0.1 M KOH, in the frequency range 100 kHz – 10 Hz. Dashed curves show the result of a simplified Randles circuit fit. The fitted capacitance increased from 0.96 µF to 13.02 µF.

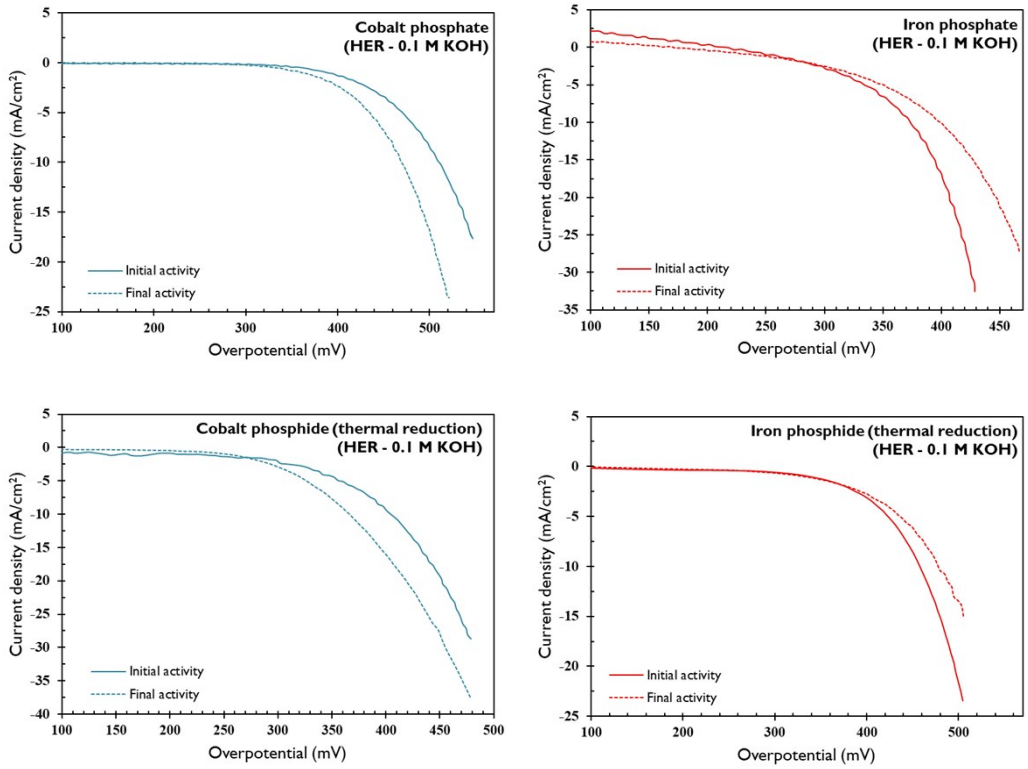

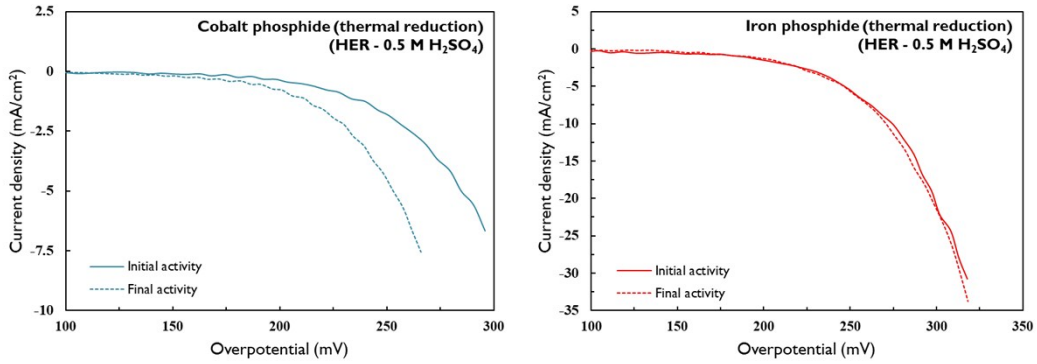

Figure S7: Cyclic voltammetry (100 mV/s) of as-deposited and thermally reduced samples in alkaline and acid conditions, before and after extended HER measurements. For HER, the 'initial activity' was defined as the first stable cyclic voltammetry after a slow staircase cyclic voltammetry, which activated some materials towards HER. Subsequent measurements included slow and fast cyclic voltammetry, chronoamperometry and chronopotentiometry, for a total measurement time of at least 12 h.

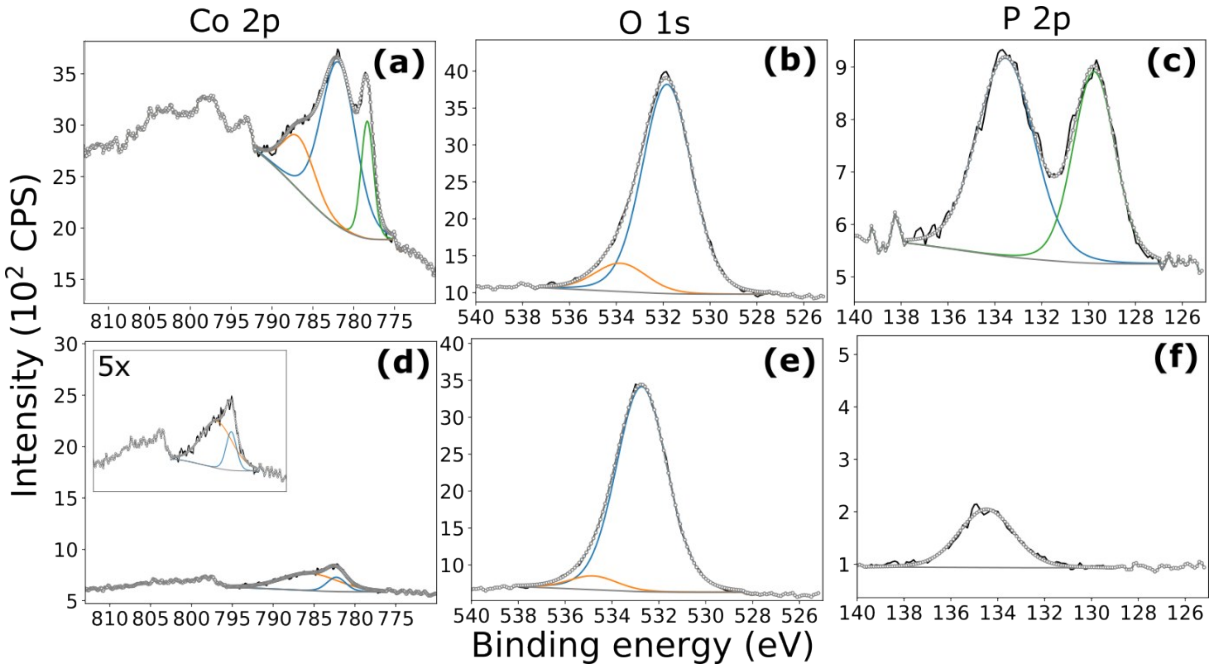

Figure S8: XPS spectra of Co 2p, O 1s and P 2p regions of as-deposited (a-c) and post-HER (in 0.1 M KOH) (d-f) cobalt phosphide material, prepared by thermal reduction. Before the reaction, metallic Co (a, 778.3 eV) and phosphide species^{-} (c, 129.8 eV) are present due to the thermal reduction process. Both these species are absent after reaction (c,f).

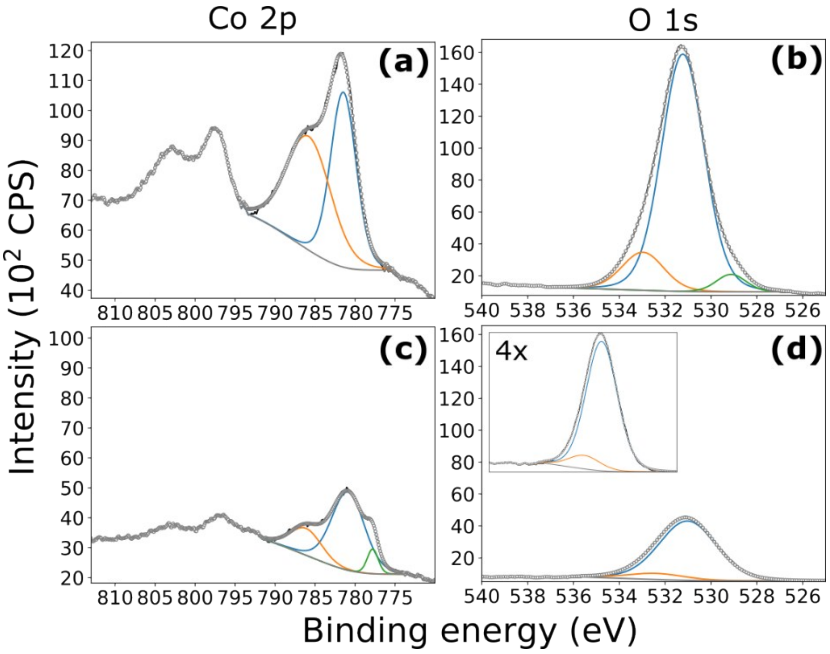

Figure S9: XPS spectra of Co 2p and O 1s regions of as-deposited (a-b) and post-HER (in 0.1 M KOH) (c-d) cobalt oxide material. Figure c shows the formation of Co at lower oxidation states, including some metallic Co (777.8 eV).

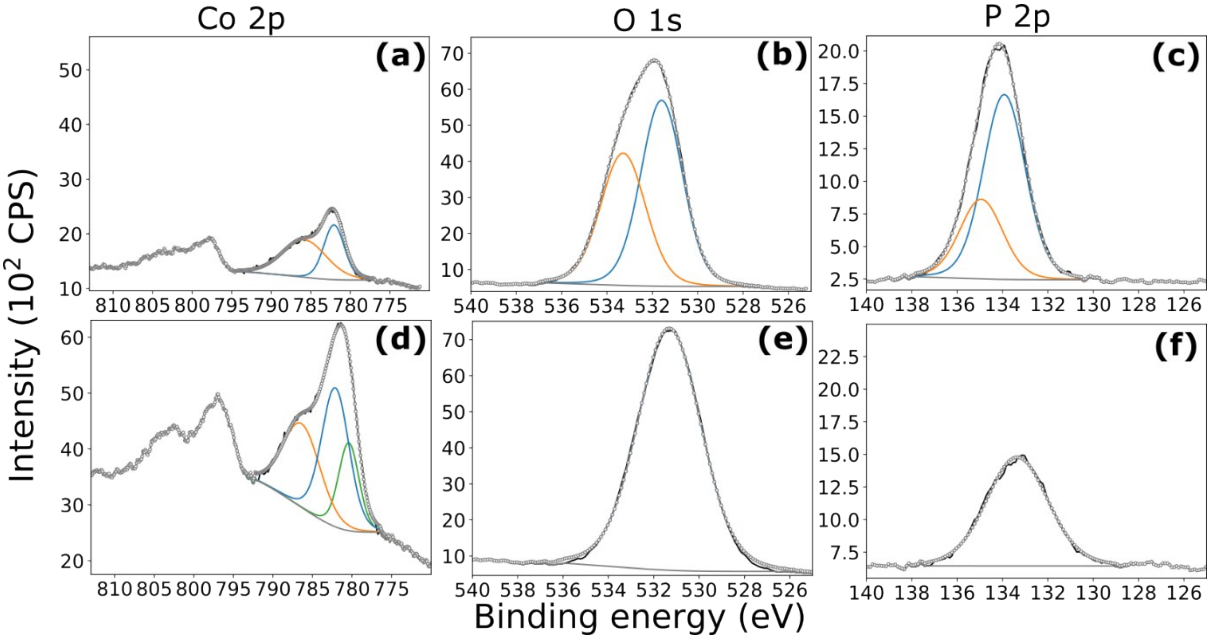

Figure S10: XPS spectra of Co 2p, O 1s and P 2p regions of as-deposited (a-c) and post-HER (in 0.1 M KOH) (d-f) cobalt phosphate material.

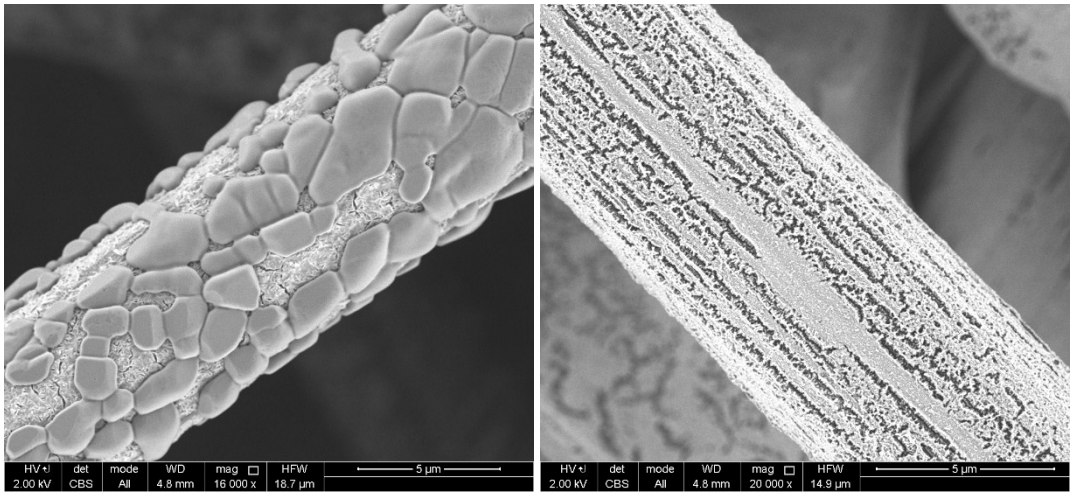

Figure S11: SEM images of as-deposited (left) and post-HER (in 0.1 M KOH) (right) cobalt phosphate material on a carbon paper electrode.

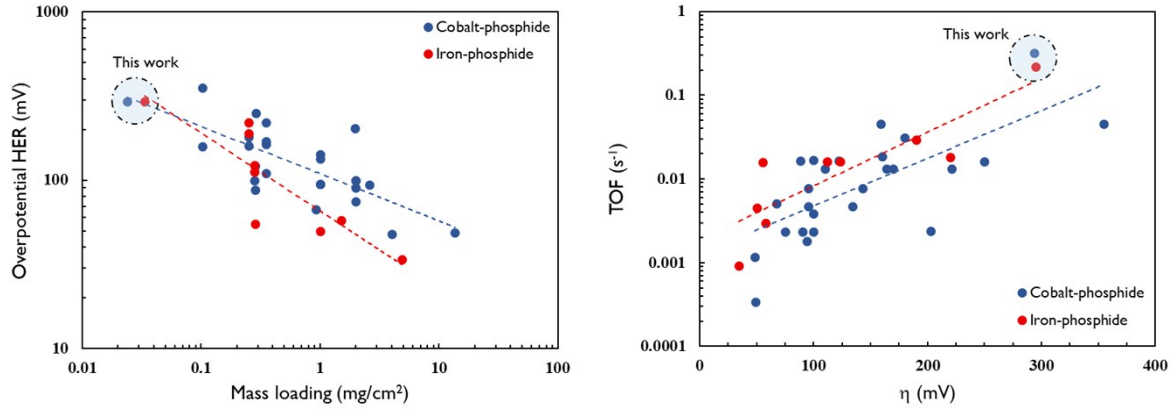

Figure S12. Mass activity data for hydrogen evolution in acid medium reported for CoP, Co_2P, FeP and Fe_2P materials (data from [10,11]). Left figure shows the required catalytic overpotential to reach a current density of 10 mA/cm^2. Right figure demonstrates Tafel behaviour when the same data are plotted as turnover frequency versus overpotential, all at a geometric current density of 10 mA/cm^2. Note that Faradaic efficiency was assumed to be 100% but not experimentally confirmed.

1 T. Dobbelaere, F. Mattelaer, J. Dendooven, P. Vereecken and C. Detavernier, *Chem. Mater.*, 2016, **28**, 3435–3445.

2 W. Knaepen, C. Detavernier, R. L. Van Meirhaeghe, J. Jordan Sweet and C. Lavoie, *Thin Solid Films*, 2008, **516**, 4946–4952.

3 W. Knaepen, S. Gaudet, C. Detavernier, R. L. Van Meirhaeghe, J. J. Sweet and C. Lavoie, *J.*

Appl. Phys., , DOI:10.1063/1.3110722.

4 G. Rampelberg, M. Schaekers, K. Martens, Q. Xie, D. Deduytsche, B. De Schutter, N. Blasco, J. Kittl and C. Detavernier, *Appl. Phys. Lett.*, 2011, **98**, 96–99.

5 J. F. Callejas, J. M. McEnaney, C. G. Read, J. C. Crompton, A. J. Biacchi, E. J. Popczun, T. R. Gordon, N. S. Lewis and R. E. Schaak, *ACS Nano*, 2014, **8**, 11101–11107.

6 N. Jiang, B. You, M. Sheng and Y. Sun, *Angew. Chemie - Int. Ed.*, 2015, **54**, 6251–6254.

7 E. J. Popczun, C. G. Read, C. W. Roske, N. S. Lewis and R. E. Schaak, *Angew. Chemie - Int. Ed.*, 2014, **53**, 5427–5430.

8 F. H. Saadi, A. I. Carim, E. Verlage, J. C. Hemminger, N. S. Lewis and M. P. Soriaga, *J. Phys. Chem. C*, 2014, **118**, 29294–29300.

9 A. Goryachev, L. Gao, Y. Zhang, R. Y. Rohling, R. H. J. Vervuurt, A. A. Bol, J. P. Hofmann and E. J. M. Hensen, *ChemElectroChem*, 2018, **5**, 1230–1239.

10 J. F. Callejas, C. G. Read, C. W. Roske, N. S. Lewis and R. E. Schaak, *Chem. Mater.*, 2016, **28**, 6017–6044.

11 J. Kibsgaard, C. Tsai, K. Chan, J. D. Benck, J. K. Nørskov, F. Abild-Pedersen and T. F. Jaramillo, *Energy Environ. Sci.*, 2015, **8**, 3022–3029.